Involvement of Iron Alkyl Complexes and Alkyl Radicals in the Kharasch Reactions: Probing the Catalysis using Iron Phosphine Complexes†

David J. Evans, Richard A. Henderson,* Adrian Hills, David L. Hughes and Kay E. Oglieve
AFRC Institute of Plant Science Research, Nitrogen Fixation Laboratory, University of Sussex, Brighton BN1 9RQ, UK

The X-ray crystal structure of *trans*-[$FeBr_2(depe)_2$] (depe = $Et_2PCH_2CH_2PEt_2$) has been determined, and its catalysis of the reactions between MgBrEt and RBr (R = Et, Pr^n, Bu^n, $PhCH_2$ or H_2CCHCH_2) to give alkanes and alkenes investigated. Detailed analysis of the products and the time courses of the reactions demonstrate that the hydrido-species *trans*-[$FeH(Br)(depe)_2]^{n+}$ (n = 0 or 1) are not intermediates in the reaction, but are products formed in the termination steps. It is shown that the catalysis can proceed by one of two pathways, depending on the alkyl halide. One pathway is proposed to involve the intermediacy of iron(I) species, and the other of iron(III) complexes. Both catalytic cycles contain the same fundamental reaction: the abstraction of a β-hydrogen atom from a $[FeEt(Br)(depe)_2]^{n+}$ species by alkyl radicals to give the alkane and ethylene. The X-ray crystal structure of *trans*-[$FeH(Br)(depe)_2$]BPh_4 is reported.

The reactions between a Grignard reagent and an alkyl halide catalysed by complexes of silver, copper, nickel or iron are known collectively as the Kharasch reactions,[1] and give rise to mixtures of alkanes and alkenes as shown in Scheme 1.

Iron complexes give the disproportionation products only, and mechanisms for this catalysis have been proposed in which the catalyst is a reduced iron species, probably iron(I).[2,3] These earlier studies used $FeCl_3$ or tris(β-diketonato)iron(III) as precursors to the catalytic species, which were generated *in situ*. Consequently, the exact nature of the catalytic species is not clear, although signals in the EPR spectrum attributable to iron(I) species have been observed in the reaction mixtures. Herein we describe structural and mechanistic studies on the reactions between MgBrEt and RBr (R = Et, Pr^n, Bu^n, $PhCH_2$ or $H_2C{=}CHCH_2$) with *trans*-[$FeBr_2(depe)_2$] (depe = $Et_2PCH_2CH_2PEt_2$) as the catalyst. Employing this species as the catalyst, in which the robust '$FeBr(depe)_2$' core is retained throughout, allows the definition of the elementary steps in the catalysis and of the intermediates involved.

Results

There are several different aspects of this study which will be presented separately, but together they define the mechanism of the catalysis presented in the Discussion section.

Hydrocarbon Products.—The yields of hydrocarbons from the reaction between MgBrEt and RBr (R = Et, Pr^n, Bu^n, $PhCH_2$ or allyl) or PhC≡CH in the presence of *trans*-[$FeBr_2(depe)_2$] with toluene as solvent are shown in Table 1. In the absence of alkyl halide only stoichiometric yields of ethane and ethylene are produced, but in the presence of the alkyl halide or phenylacetylene catalysis is clearly evident. The extent of the catalysis is not great, being at best between 10 and 16 turnovers, which is about an order of magnitude less than that observed with $FeCl_3$.[2] This does not detract from our prime objective in this study: to define the elementary steps in the catalysis. In none of these studies was any butane observed. In the studies with allyl bromide the amount of ethylene is significantly higher than the amount of ethane. However, a significant proportion of propene (derived from the allyl bromide) is observed in this reaction, and the sum of the amounts of ethane and propene is close to the amount of ethylene. The reaction products from the catalysis with $PhCH_2Br$ have not been determined since the expected toluene product would not be distinguishable from the solvent. If the alkyl bromide is replaced by phenylacetylene little ethylene is produced, and the predominant product is ethane. The complexes *trans*-[$FeH(Br)(depe)_2]^{n+}$ (n = 0 or 1) also catalyse the reaction between MgBrEt and EtBr as shown in Table 1, but with a product distribution different from that observed with *trans*-[$FeBr_2(depe)_2$].

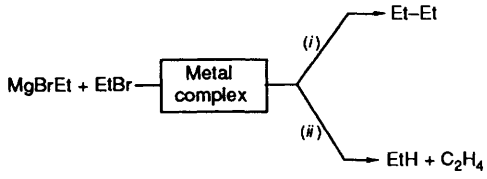

Scheme 1 Reactions between MgBrEt and EtBr catalysed by metal complexes. (*i*) Combination; (*ii*) disproportionation

Time Course for the Evolution of Hydrocarbons.—The production of the hydrocarbon gases was monitored over the first 2 h as shown in Fig. 1 for RBr (R = Et, Pr^n or allyl). Over protracted times formation of *trans*-[$FeH(Br)(depe)_2]^{n+}$ occurs (with a change of hydrocarbon product distribution) and this complicates any detailed kinetic analysis, which was therefore not undertaken.

Nonetheless, it is clear that the initial rate of hydrocarbon production for RBr (R = Et, Pr^n or Bu^n) exhibits a simple first-order dependence on the concentration of *trans*-[$FeBr_2(depe)_2$] ([Fe] = 2–16 mmol dm^{-3}) and is independent of the concentration of MgBrEt (40–160 mmol dm^{-3}) and the concentration and nature of alkyl bromide ([RBr] = 40–320 mmol dm^{-3}). The time course for the production of hydrocarbons in the reactions with allyl bromide also shows an initial rate which depends on the concentration of *trans*-[$FeBr_2(depe)_2$] alone, over the concentration ranges itemised above. However, the initial rate is

† *Supplementary data available:* see Instructions for Authors, *J. Chem. Soc., Dalton Trans.*, 1992, Issue 1, pp. xx–xxv.

Table 1 Yields and product distribution of hydrocarbons upon the cessation of catalysis

	Amount of reactant/mmol			Amount of product/mmol		
Complex[a]	MgBrEt	EtBr	Other	C_2H_6	C_2H_4	Other[b]
$[FeBr_2(depe)_2]$	1.0			0.12	0.10	
	3.0	3.0		1.10	1.10	
	5.0	5.0		1.60	1.60	
	2.0		2.0 (Pr^nBr)	1.60	1.60	0.15 (C_3H_6), 0.10 (C_3H_8)
	2.0		2.0 (Bu^nBr)	0.80	0.80	0.012 (C_4H_8), 0.024 (C_4H_{10})
	2.0		1.0 (C_3H_5Br)	0.23	0.81	0.39 (C_3H_6)
	2.0		1.0 (PhCCH)	0.70	0.18	
$[FeH(Br)(depe)_2]$	1.0			0.12	0.01	
	1.0	1.0		0.58	0.25	
	1.0		1.0 (Pr^nBr)	0.61	0.22	0.015 (C_3H_6), 0.064 (C_3H_8)
$[FeH(Br)(depe)_2]BPh_4$	1.0	1.0		0.74	0.35	
	1.0			0.13	0.05	

[a] 0.1 mmol Fe. [b] Increased solubilities of these gases, compared to C_2H_6 and C_2H_4, means that the amounts given do not represent the true amounts.

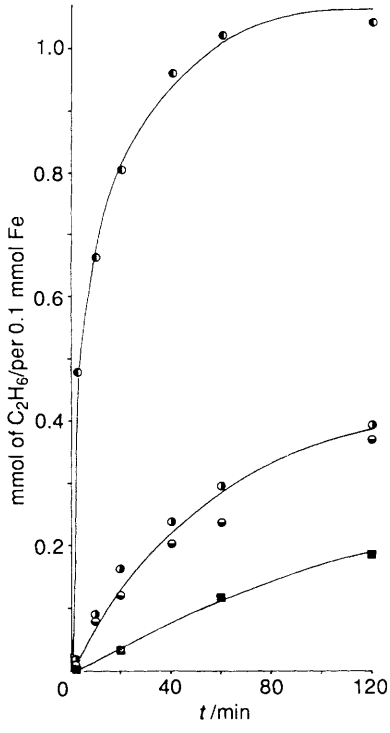

Fig. 1 Time courses for the production of ethane from the reaction of MgBrEt with RBr in the presence of iron complexes at 20 °C in toluene: *trans*-$[FeBr_2(depe)_2]$, R = allyl (◐), Et (◑) or Pr^n (◒); *trans*-$[FeH(Br)(depe)_2]$, R = Pr^n (■). In all cases identical data are obtained when the concentration of iron complex is varied over the range 2–16 mmol dm^{-3}, that of MgBrEt over the range 40–160 mmol dm^{-3} or that of alkyl bromide over the range 40–320 mmol dm^{-3}

an order of magnitude greater as shown in Fig. 1. In a less detailed study the rate of production of hydrocarbons by *trans*-$[FeH(Br)(depe)_2]$ has been shown to be much slower than is observed for *trans*-$[FeBr_2(depe)_2]$, again shown in Fig. 1.

Iron Products of Catalysis.—The low turnover number in the catalysis by *trans*-$[FeBr_2(depe)_2]$ is, at least in part, due to intermediates undergoing secondary reactions resulting in poorly catalytic species. Depending on the nature of the alkyl bromide, one of three products is formed. The analytical and spectroscopic characterisation of these products is shown in Table 2.

In the presence of RBr (R = Et, Pr^n or Bu^n), or with no alkyl bromide present, *trans*-$[FeH(Br)(depe)_2]$ is obtained. In the presence of R′Br (R′ = $PhCH_2$ or allyl), and after subsequent

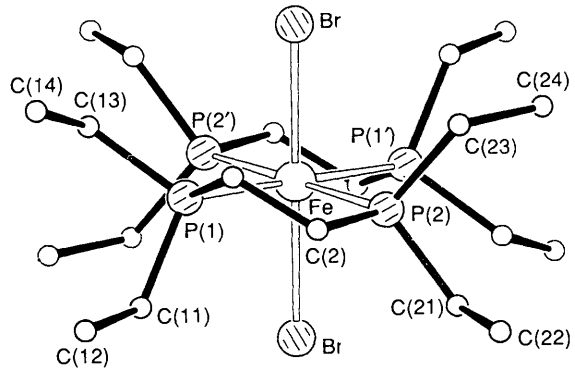

Fig. 2 Molecular structure of *trans*-$[FeBr_2(depe)_2]$, showing the atomic numbering scheme

work-up with $NaBPh_4$, *trans*-$[FeH(Br)(depe)_2]BPh_4$ was isolated and identified by an X-ray crystal structure analysis and by comparison of its spectroscopic properties with those of *trans*-$[FeH(Cl)(dppe)_2]^+$ (dppe = $Ph_2PCH_2CH_2PPh_2$).[6] In particular the species *trans*-$[FeH(X)(L\text{–}L)_2]^+$ (L–L = diphosphine) show a weak band in the IR spectrum at 1860 cm^{-1} attributable to ν(FeH).

In the presence of phenylacetylene, *trans*-$[Fe(CCPh)Br(depe)_2]$ is the product.

The Mössbauer spectrum of each product has been measured and the parameters are listed in Table 2.

During the course of this study we also determined the X-ray crystal structures of *trans*-$[FeBr_2(depe)_2]$ and *trans*-$[FeH(Br)(depe)_2]BPh_4$.

Structure of trans-$[FeBr_2(depe)_2]$.—The X-ray crystal structure of *trans*-$[FeBr_2(depe)_2]$ is shown in Fig. 2. The principal dimensions are given in Table 3 and the atomic coordinates are listed in Table 4.

This compound is isostructural with, and essentially identical to, *trans*-$[FeI_2(depe)_2]$,[7] and completes the series of structures for *trans*-$[FeX_2(depe)_2]$ (X = Cl, Br or I).[8,9] In each the iron atom lies on a centre of symmetry and is surrounded by the four phosphorus atoms in a rectangular co-ordination plane; the two mutually *trans* halide ligands, almost normal to the P_4 plane, complete the octahedral co-ordination pattern.

Structure of trans-$[FeH(Br)(depe)_2]BPh_4$.—The X-ray crystal structure of the cation is shown in Fig. 3. The principal dimensions of the cation are given in Table 5 and the atomic coordinates are listed in Table 6. The data are of sufficiently high quality that the hydrido-ligand could be located. From X-ray analyses, Fe–H distances have been recorded for several octahedral iron(II) complexes, *e.g.*

Table 2 Analytical and spectroscopic characterisation of iron complexes

Complex	Colour	Elemental analysis (%)[a] C	H	IR (cm^{-1})	NMR (δ) ^{1}H[b]	^{31}P[c]	Mossbauer/mm s^{-1} Isomer shift exptl.	calc.	Quadrupole splitting exptl.	calc.[d]	Γ
$[FeBr_2(depe)_2]$	Light green	38.3 (38.2)	7.4 (7.6)			−74.1[e]	0.47	0.45	1.51	+1.48	0.18[f]
$[FeH(Br)(depe)_2]$	Orange	43.3 (43.7)	9.1 (8.9)	1840w ν(FeH)	−30.9(1) [1, J(PH) = 49 Hz]	−55.3[g]	0.22	0.25	0.15	−0.16	0.23
$[Fe(CCPh)Br(depe)_2]$	Orange	51.8 (51.8)	8.1 (8.2)	2160s ν(C≡C)	6.4–6.7(5) (m, Ph)	−70.5			[h]		
$[FeH(Br)(depe)_2]BPh_4$	Red	61.5 (60.8)	7.9 (7.8)	1880w ν(FeH)			0.22	—	2.14	—	0.26[i]

[a] Calculated values shown in parentheses. [b] Shifts referred to $SiMe_4$. All spectra show unresolved peaks at δ 0.87 (CH_3CH_2), 1.21–1.61 (CH_3CH_2) and 2.0 (CH_2CH_2). [c] Shifts referred to trimethyl phosphite. [d] Calculated using partial isomer shifts and partial quadrupole splitting (H = 0.00) parameters as defined in ref. 4. [e] Very broad. [f] In good agreement with the values reported earlier.[5] [g] Proton undecoupled spectrum is a doublet J(PH) = 43.6 Hz. [h] Previously reported in ref. 4. [i] Consistent with a low-spin iron(III) complex.

Table 3 Principal bond dimensions (distances in Å, angles in °) in *trans*-$[FeBr_2(depe)_2]$ with estimated standard deviations (e.s.d.s) in parentheses

(*a*) About the iron atom

Fe–Br	2.509(1)	Br–Fe–P(1)	85.70(2)
Fe–P(1)	2.280(1)	Br–Fe–P(2)	88.97(2)
Fe–P(2)	2.300(1)	P(1)–Fe–P(2)	83.62(3)

(*b*) Torsion angle in the depe ligand

P(1)–C(1)–C(2)–P(2) 50.4(4)

Table 4 Final atomic coordinates (fractional × 10^4) for *trans*-$[FeBr_2(depe)_2]$ with e.s.d.s in parentheses

Atom	x	y	z
Fe	0	0	0
Br	−2189.1(6)	1659.0(6)	1.5(5)
C(11)	4061(6)	1642(6)	2271(5)
C(12)	5535(8)	2974(8)	3072(8)
C(13)	1032(7)	2596(6)	3064(5)
C(14)	1900(9)	4228(6)	3825(6)
P(1)	1853(1)	1927(1)	1612(1)
C(1)	2470(6)	3719(5)	855(4)
C(2)	3063(7)	3258(6)	−408(4)
P(2)	1367(1)	1535(1)	−1405(1)
C(21)	2709(6)	771(6)	−2472(5)
C(22)	3895(8)	1938(7)	−3144(6)
C(23)	96(7)	2577(6)	−2515(5)
C(24)	−1121(8)	1598(7)	−3742(5)

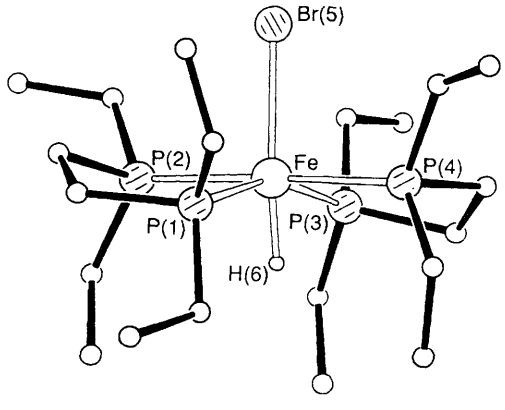

Fig. 3 Structure of the cation in *trans*-$[FeH(Br)(depe)_2]BPh_4$, with a numbering scheme similar to that shown in Fig. 2

Table 5 Principal molecular dimensions (distances in Å, angles in °) in *trans*-$[FeH(Br)(depe)_2]BPh_4$ with e.s.d.s in parentheses

(*a*) About the iron atom

Fe–P(1)	2.299(2)	Fe–P(4)	2.269(2)
Fe–P(2)	2.278(2)	Fe–Br(5)	2.415(1)
Fe–P(3)	2.261(2)	Fe–H(6)	1.35(5)
P(1)–Fe–P(2)	83.8(1)	P(3)–Fe–Br(5)	99.7(1)
P(1)–Fe–P(3)	158.4(1)	P(4)–Fe–Br(5)	91.6(1)
P(2)–Fe–P(3)	95.5(1)	P(1)–Fe–H(6)	87.1(20)
P(1)–Fe–P(4)	95.0(1)	P(2)–Fe–H(6)	90.1(21)
P(2)–Fe–P(4)	177.9(1)	P(3)–Fe–H(6)	71.3(20)
P(3)–Fe–P(4)	85.0(1)	P(4)–Fe–H(6)	88.0(21)
P(1)–Fe–Br(5)	101.9(1)	Br(5)–Fe–H(6)	171.0(20)
P(2)–Fe–Br(5)	90.4(1)		

(*b*) Torsion angles in the depe ligands

P(1)–C(1)–C(2)–P(2) 34.8(10)
P(3)–C(3)–C(4)–P(4) 42.5(13)

$[FeH(H_2)(dppe)_2]BF_4$ [1.28(8)],[10] $[FeH(H_2)(dppe)_2]BPh_4$ [1.30(3)],[11] $[FeH(N_2)(dmpe)_2]BPh_4$ (dmpe = $Me_2PCH_2CH_2PMe_2$) [(mean of two) 1.32(2)][12] and $[FeH(N_2)(Ph_2PCH_2CH_2PPhCH_2CH_2PPhCH_2CH_2PPh_2)]Br$ [1.53(9) Å];[13] a neutron study at 20 K of $[FeH(H_2)(dppe)_2]BPh_4$ yielded Fe–H 1.535(12) Å.[11] Our distance of 1.35(5) Å falls in the centre of this wide range of values. Further comparison of these dimensions is inappropriate here, bearing in mind the different oxidation states of the metal and the nature of the *trans* ligand, and the lack of precision in the dimensions.

The most significant feature in the cation is in its deviation from octahedral co-ordination geometry. The four phosphorus atoms form a shallow tetrahedron, of depth 0.39 Å. The iron atom lies close to the top edge, P(2) · · · P(4), of this tetrahedron so that the two remaining P atoms, P(1) and P(3), appear displaced towards the hydride ligand. A similar arrangement of P atoms was noted in the two distinct cations of $[FeH(N_2)(dmpe)_2]BPh_4$, where the tetrahedron has a depth of *ca.* 0.10 Å and the Fe atom is *ca.* 0.18 Å from the centre of that body and away from the hydride ligand.[12] The difference in size of the *trans* ligands is less here than in the bromo hydride complex, and the oxidation state of the metal atom is lower, hence the distortion from a regular octahedral pattern is less marked in the dinitrogen complex. We note that in both these complexes the *gauche* P–C–C–P torsion angles in the two diphosphine ligands in each complex are of the same sign. In the production of $[FeH(Br)(depe)_2]BPh_4$ from the dibromo compound, therefore, one of the diphosphine ligands has inverted, changing its

Table 6 Final atomic coordinates (fractional × 10^4) for *trans*-[FeH(Br)(depe)$_2$]BPh$_4$ with e.s.d.s in parentheses

Atom	*x*	*y*	*z*	Atom	*x*	*y*	*z*
Fe	921.9(9)	1060.9(6)	827.2(3)	B(7)	3745(7)	6562(5)	1628(3)
P(1)	1123(2)	988(1)	1712.1(7)	C(71a)	3400(6)	5693(4)	1928(3)
C(11)	2593(7)	781(6)	2018(3)	C(72a)	3418(7)	5632(5)	2463(3)
C(12)	3553(10)	1464(9)	1951(5)	C(73a)	3229(8)	4877(6)	2728(3)
C(13)	136(7)	264(5)	2043(3)	C(74a)	2994(9)	4173(6)	2442(5)
C(14)	−4(10)	379(7)	2634(3)	C(75a)	2958(8)	4201(5)	1923(5)
C(1)	626(13)	1977(5)	1994(4)	C(76a)	3155(7)	4948(5)	1673(3)
C(2)	493(10)	2622(6)	1634(3)	C(71b)	5232(6)	6572(4)	1528(2)
P(2)	−62(2)	2275(1)	1002.3(7)	C(72b)	5957(7)	5874(4)	1563(2)
C(21)	−1717(8)	2332(6)	1056(3)	C(73b)	7215(8)	5885(6)	1452(3)
C(22)	−2357(8)	1740(6)	1407(5)	C(74b)	7817(8)	6579(8)	1324(3)
C(23)	265(9)	3172(4)	591(4)	C(75b)	7116(8)	7315(7)	1283(3)
C(24)	−96(11)	4016(5)	792(4)	C(76b)	5855(8)	7305(6)	1388(3)
P(3)	70(2)	879(1)	37.5(7)	C(71c)	3014(6)	6632(4)	1070(2)
C(31)	638(9)	1603(6)	−441(3)	C(72c)	3521(7)	6991(4)	627(3)
C(32)	292(12)	1486(7)	−993(3)	C(73c)	2885(8)	7118(4)	171(3)
C(33)	−1591(8)	913(6)	−66(4)	C(74c)	1670(8)	6868(5)	140(3)
C(34)	−2337(10)	286(7)	231(5)	C(75c)	1120(7)	6501(5)	563(3)
C(3)	399(16)	−157(9)	−177(5)	C(76c)	1801(7)	6382(5)	1004(3)
C(4)	1580(19)	−445(8)	8(4)	C(71d)	3309(6)	7355(4)	1994(2)
P(4)	1852(2)	−174(1)	672.5(8)	C(72d)	4103(8)	7804(4)	2292(3)
C(41)	1446(8)	−1082(5)	1035(3)	C(73d)	3716(9)	8465(5)	2616(3)
C(42)	92(10)	−1315(6)	1025(4)	C(74d)	2513(10)	8647(5)	2650(3)
C(43)	3584(13)	−182(10)	710(9)	C(75d)	1695(8)	8201(5)	2365(3)
C(44)	4298(16)	−622(12)	706(10)	C(76d)	2084(7)	7560(4)	2049(2)
Br(5)	2741.3(8)	1817.2(6)	583.3(4)				
H(6)	−136(49)	643(30)	884(18)				

torsion angle sign, since the dibromo-complex molecule is centrosymmetric and its two diphosphine ligands have opposite conformations. The oxidation state of the iron and the co-ordination distortions in the bromo hydride complex allow a shortening of the Fe–Br distance to 2.415(1) from 2.509(1) Å in the dibromide complex (see above). The Fe–P distances are less affected, shortening slightly from a mean value of 2.290(10) Å in the dibromo complex to 2.277(8) Å in the bromo hydride.

The anion in [FeH(Br)(depe)$_2$]BPh$_4$ is well resolved and linked to the cations only by normal van der Waals interactions.

Discussion

To establish the elementary reactions for any catalysis is difficult because of the large number of steps under investigation, and because only the rate-limiting step is amenable to kinetic elucidation. The use of structurally well characterised catalysts is fundamental to any investigation of their reactivity, and the use in this study of the system based on the robust 'FeBr(depe)$_2$' core is central to this theme. Previous studies [1–3] on the Kharasch reactions catalysed by iron complexes employed 'catalyst precursors' such as $FeCl_3$ which are structurally poorly defined and hence preclude detailed understanding of the action of the catalyst. These previous studies indicated the mechanism shown in equations (1)–(4),

$$Fe^{II}\text{–}Br + MgBrEt \longrightarrow Fe^{II}\text{–}Et + MgBr_2 \quad (1)$$

$$2Fe^{II}\text{–}Et \longrightarrow 2Fe^{I} + C_2H_6 + C_2H_4 \quad (2)$$

$$Fe^{I} + EtBr \longrightarrow Fe^{II}Br + Et^{\bullet} \quad (3)$$

$$Fe^{I} + Et^{\bullet} \longrightarrow Fe^{II}\text{–}Et \quad (4)$$

with step (3) being rate-limiting, consistent with the first-order dependence on the concentration of alkyl halide observed in these earlier studies.

This mechanism is inconsistent with the observations made in the present study for the following reasons. First, the formation, and implied intermediacy, of iron(III) species in reactions with $PhCH_2Br$ or H_2CCHCH_2Br, and secondly the rate of all our reactions are independent of the concentration of MgBrEt or EtBr. Previously, it has been proposed [14] tentatively that the intimate mechanism of step (2) involves an intramolecular β-hydride abstraction reaction and the intermediacy of hydrido-species as shown in equations (5) and (6). Independent studies

$$Fe^{II}\text{–}Et \longrightarrow Fe^{II}H + C_2H_4 \quad (5)$$

$$Fe^{II}H + Fe^{II}\text{–}Et \longrightarrow 2Fe^{I} + C_2H_6 \quad (6)$$

on *trans*-[FeH(Br)(depe)$_2$] [the putative hydrido-intermediate in equations (5) and (6)] demonstrate that these species are *not* intermediates in the catalysis. This conclusion is based on the hydrocarbon product distribution (Table 1), which differs from that with *trans*-[FeBr$_2$(depe)$_2$], and the slower rate of production of hydrocarbons (Fig. 1). We observe that, rather than being intermediates in the catalysis, hydrido-complexes are products formed in termination steps of the catalysis. The sequence of reactions shown in Scheme 2 is consistent with all the mechanistic information concerning the reactions of MgBrEt and alkyl bromides in the presence of *trans*-[FeBr$_2$(depe)$_2$].

Thus we propose that there are two catalytic cycles, one involving iron(I) and the other involving iron(III) intermediates. The left-hand cycle, involving iron(I) species, operates with RBr (R = Et, Pr^n or Bu^n) and is similar to that described in equations (1)–(4).[2] The key difference is our conclusion that ethyl radicals abstract a β-hydrogen atom from *trans*-[FeEt(Br)(depe)$_2$] to give ethane and *trans*-[Fe(η^2-C_2H_4)Br(depe)$_2$]. Subsequent dissociation of the ethylene to give [FeBr(depe)$_2$] is the rate-limiting, unimolecular step. The iron(I) species thus formed abstracts a bromine atom from RBr, thus completing the catalytic cycle and regenerating the alkyl radical. The proposal that the rate-limiting step in the catalysis is the dissociation of the ethylene from *trans*-[Fe(η^2-C_2H_4)Br(depe)$_2$] is consistent with the rate of hydrocarbon production, being independent of the concentration and the nature of the alkyl bromide. The conclusion that alkyl radicals abstract β-hydrogen atoms from ethyl ligands avoids the intermediacy of hydrido-species during the catalysis. Such abstraction reactions

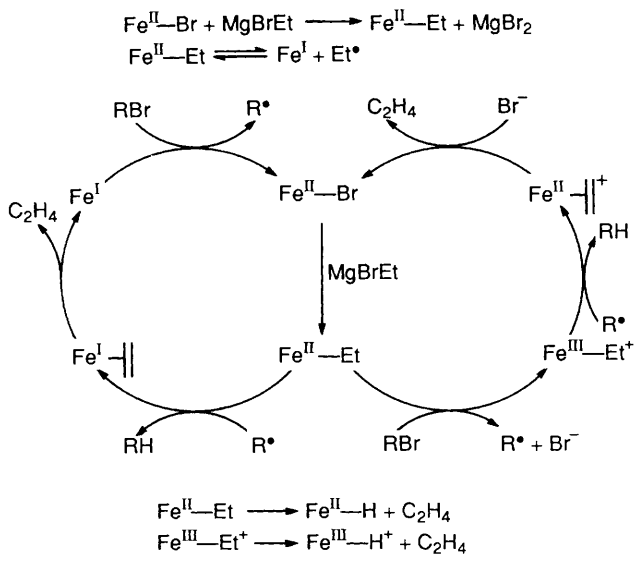

Scheme 2 Mechanistic pathways for the *trans*-[$FeBr_2(depe)_2$] catalysis of the reaction between MgBrEt and RBr (R = Et, Pr^n or Bu^n operates by the left-hand cycle, R = $PhCH_2$ or H_2CCHCH_2 by the right-hand cycle), to give alkane and alkene

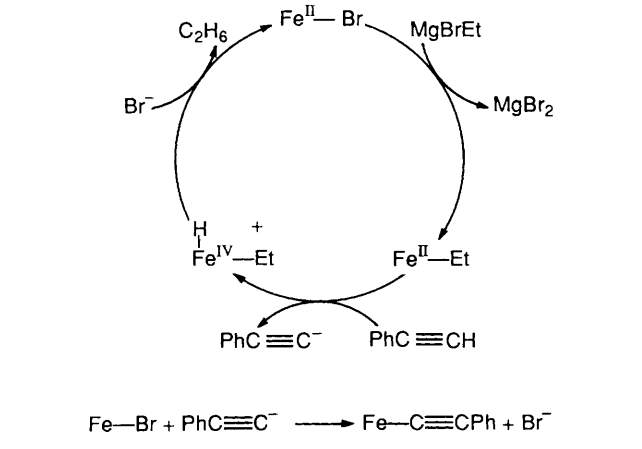

Scheme 3 Mechanistic pathway for the *trans*-[$FeBr_2(depe)_2$] catalysis of the reaction between MgBrEt and PhCCH to give ethane

are known at other metals.[15,16] It has been argued[1,2,14] that free radicals cannot be involved in the iron-catalysed reactions between MgBrEt and EtBr since [based on the ratio of the rate constants for radical combination (k_c) and disproportionation (k_d), k_c/k_d = *ca.* 6] it would be expected that appreciable amounts of butane would result. This argument is only valid in the absence of other potential reactants. However, it is just the basis of the catalytic cycles in Scheme 2 that the ethyl iron complexes represent species which can rapidly scavenge alkyl radicals. To initiate the catalysis for the left-hand cycle there must be a source of alkyl radicals. It is proposed that homolysis of the iron–carbon bond generates the alkyl radical, and such homolyses are well known in a variety of metal complexes.[17] The left-hand cycle cannot explain the formation of the iron(III) species, *trans*-[$FeHBr(depe)_2$]$^+$, in the reactions involving the so-called 'activated' alkyl bromides, $PhCH_2Br$ or H_2CCHCH_2Br. Furthermore, the reactions with these alkyl bromides are markedly faster than those with RBr (R = Et, Pr^n or Bu^n). These observations are consistent with another catalytic cycle, shown on the right-hand side of Scheme 2. This pathway employs the same initial alkylation of *trans*-[$FeBr_2(depe)_2$] by MgBrEt as operates in the left-hand cycle, but, with the 'activated' alkyl bromides, electron transfer from *trans*-[FeEt(Br)(depe)$_2$] can successfully compete with the attack by the low concentration of ethyl radicals formed by the initiation homolysis. Subsequent β-hydrogen abstraction from the derived *trans*-[$FeEt(Br)(depe)_2$]$^+$ by the alkyl radical gives the alkane and *trans*-[$Fe(\eta^2\text{-}C_2H_4)Br(depe)_2$]$^+$. Dissociation of the ethylene from this species is the rate-limiting step, analogous to that observed in the left-hand cycle. This is consistent with (*i*) the independence of the initial rate of hydrocarbon production on the concentration of alkyl bromide or MgBrEt and (*ii*) the increased initial rate of the reaction with H_2CCHCH_2Br over that with the simple alkyl bromides. Capture of [$FeBr(depe)_2$]$^+$, formed upon dissociation of ethylene, by bromide ion completes the catalytic cycle.

The pathways shown in Scheme 2 are consistent with two mechanistic conclusions concerning this general type of reaction, which were established in earlier studies. First, iron(I) species are involved in the catalysis[1,2,14] and secondly the alkyl radicals are derived entirely from the alkyl halide.[2,3] With respect to this last point, the catalytic cycles shown in Scheme 2 may be a little misleading. In the iron(I) cycle the alkyl radical released from RBr may not have time to react with *trans*-[FeEt(Br)(depe)$_2$] before it is captured by the excess of MgBrEt according to equation (7). This exchange reaction has

$$R^\bullet + MgBrEt \longrightarrow Et^\bullet + MgBrR \qquad (7)$$

been observed in similar systems to those described here.[1] Such exchanges may complicate the quantitative analysis of the hydrocarbon products in the reactions with Pr^nBr (Table 1). In the studies with H_2CCHCH_2Br it is clear from the product analysis (Table 1) that MgBrEt does not efficiently scavenge the allyl radical and so propene is formed in significant amounts. The termination steps in both cycles appear to be the formation of *trans*-[$FeH(Br)(depe)_2$]$^{n+}$ from the corresponding *trans*-[$FeEt(Br)(depe)_2$]$^{n+}$ by intramolecular β elimination of ethylene.

Finally, in the presence of phenylacetylene the predominant hydrocarbon product is ethane. It is proposed that this catalysis involves the pathway shown in Scheme 3. Here we propose phenylacetylene is acting as a mild proton source, which effectively intercepts *trans*-[$FeBr_2(depe)_2$] to give ethane, possibly *via* the ethyl hydride species. The termination step in this catalytic cycle occurs when *trans*-[$FeBr_2(depe)_2$] reacts preferentially with the increasing concentration of phenyl acetylide to give *trans*-[$Fe(CCPh)Br(depe)_2$]. There has been no attempt to determine the time course for ethane production in this system since the appreciable amount of ethylene present indicates that even in the presence of a large excess of phenylacetylene there appears to be 'leakage' into the iron(I) cycle.

Conclusion

We have shown that the reactions between MgBrEt and RBr catalysed by *trans*-[$FeBr_2(depe)_2$] can occur by two pathways. The first, involving iron(I) intermediates, is that adopted by simple alkyl bromides (R = Et, Pr^n or Bu^n), and the second, involving iron(III) intermediates, operates only with the so-called 'activated' alkyl bromides (R = $PhCH_2$ or H_2CCHCH_2). Both pathways are consistent with the mechanistic criteria established in this study, namely: (*i*) hydrido-species are not intermediates in the catalysis, (*ii*) the initial rates of hydrocarbon production are independent of the concentrations of alkyl bromide or MgBrEt and (*iii*) the formation of iron(III) products in the reactions with 'activated' alkyl bromides. In addition, the two catalytic cycles are consistent with the mechanistic criteria established in earlier studies[1–3,14] that (*iv*) iron(I) species are involved in the catalysis and (*v*) alkyl radicals are derived from RBr only. We do not pretend that these are the only two pathways that can operate in these reactions, and in at least one case chemically induced dynamic nuclear polarisation experiments[3] have identified a pathway involving bimolecular

reactions of alkyl radicals, but others have indicated that this probably only represents a minor pathway.[1]

Experimental

All manipulations were performed under an atmosphere of argon using standard Schlenk-tube and syringe techniques as appropriate. All solvents were freshly distilled from an appropriate drying agent immediately prior to use. Anhydrous $FeBr_2$ (Aldrich) was used as received and *trans*-$[FeBr_2(depe)_2]$[8] and depe[18] were prepared by the literature methods. The Grignard reagent, MgBrEt, was prepared and standardised by the methods described earlier.[2] Infrared spectra were recorded on a Perkin-Elmer 883 spectrophotometer, ^1H and ^{31}P NMR spectra on a JEOL GSX 270 spectrometer. The Mössbauer spectra were determined on an ES Technology MS-105 spectrometer with a 25 mCi ^{57}Co source in a rhodium matrix. Spectra were recorded at 77 K and referenced against iron foil at 298 K. Gas composition and concentrations were determined using a Philips PU440 gas–liquid chromatograph and computing integrator PU4815 equipped with a Poropak Q column at 130 °C. The gases were identified and amounts calculated after calibration of the machine with known concentrations of authentic samples of each gas: ethane, ethylene, propane, propene, butane and but-1-ene.

Isolations.—trans-*Bis*[1,2-*bis*(*diethylphosphino*)*ethane*]-*bromohydridoiron.* To a solution of *trans*-$[FeBr_2(depe)_2]$ (0.55 g, 0.88 mmol) in toluene (*ca.* 25 cm^3) was added RBr (8.8 mmol) and then MgBrEt (1.4 g, 8.8 mmol). There was an immediate colour change to orange, and the solution was stirred for 18 h to ensure complete formation of the hydrido-product. Methanol was slowly added dropwise, just sufficient to destroy the excess of Grignard reagent. The magnesium salts were removed by filtration, and the filtrate concentrated to dryness to give a sticky orange residue. This was extracted into boiling hexane (*ca.* 25 cm^3), filtered through Celite, then left at −20 °C overnight to produce orange needles of the product. Concentration of the solution produced further crops of the compound. Yield = 0.40 g (85%).

trans-*Bis*[1,2-*bis*(*diethylphosphino*)*ethane*]*bromo*(*phenylethynyl*)*iron.* This compound was prepared in an analogous manner to that described above using *trans*-$[FeBr_2(depe)_2]$ (0.55 g, 0.88 mmol) in toluene (*ca.* 25 cm^3) with phenylacetylene (0.82 g, 8.0 mmol) and MgBrEt (1.27 g, 8 mmol). Yield = 0.40 g (70%).

trans-*Bis*[1,2-*bis*(*diethylphosphino*)*ethane*]*bromohydridoiron tetraphenylborate.* To a solution of *trans*-$[FeBr_2(depe)_2]$ (0.55 g, 0.88 mmol) in toluene (*ca.* 25 cm^3) was added RBr (R = $PhCH_2$ or H_2CCHCH_2) (8 mmol) and then MgBrEt (1.27 g, 8 mmol). There was an immediate formation of an orange colour, and the solution was stirred for 1 h. Methanol was added dropwise to destroy the excess of Grignard reagent. The magnesium salts were removed by filtration, and the filtrate concentrated to dryness *in vacuo*. The residue was dissolved in the minimum of methanol (*ca.* 25 cm^3), filtered through Celite and then addition of $NaBPh_4$ (0.34 g, 10 mmol) produced a red solid. The product was recrystallised from dichloromethane–diethyl ether as red cubes. Yield = 0.62 g (82%).

Analysis of the Hydrocarbon Distribution in the Reactions of MgBrEt *with* RBr *in the Presence of trans*-$[FeBr_2(depe)_2]$.—In a typical experiment, a round-bottomed flask (500 cm^3) was loaded with *trans*-$[FeBr_2(depe)_2]$ (0.063 g, 0.1 mmol) in toluene (25 cm^3) and EtBr (0.22 g, 2.0 mmol) under an atmosphere of argon. The flask was immersed in a thermostatted tank at 20 °C and sealed by closing the Jencons gas-tight tap. The MgBrEt (0.26 g, 2.0 mmol) was injected through a rubber septum using a hypodermic syringe. Gas samples (volume = 0.1 cm^3) were taken at required intervals and analysed by GLC.

Crystal Structure Analyses.—*trans*-$[FeBr_2(depe)_2]$. *Crystal data.* $C_{20}H_{48}Br_2FeP_4$, M = 628.2, triclinic, space group $P\bar{1}$ (no. 2), a = 7.8355(7), b = 8.8045(8), c = 10.3412(11) Å, α = 95.602(8), β = 99.737(8), γ = 104.070(8)°, U = 674.8 $Å^3$, Z = 1, D_c = 1.546 g cm^{-3}, $F(000)$ = 324, μ(Mo-Kα) = 37.3 cm^{-1}, λ(Mo-Kα) = 0.710 69 Å.

Crystals are yellow parallelopipeds. One, *ca.* 0.29 × 0.17 × 0.12 mm, was mounted on a glass fibre and, after preliminary photographic examination, was transferred to our Enraf-Nonius CAD4 diffractometer (with monochromated radiation). Accurate cell parameters were refined from the goniometer settings of 25 strong reflections with θ *ca.* 10.5°, each centred in four orientations. Diffraction intensities were measured for the $(+h,\pm k,\pm l)$ reflections to θ_{max} = 25°. During processing the data were corrected for Lorentz polarisation effects, slight deterioration of the crystal (6.0% during the data collection), absorption (from ψ-scan measurements) and to ensure no negative net intensities (by Bayesian statistical methods). 2376 Unique data were entered into the SHELX progam system[19] for structure determination (by the heavy-atom method) and refinement (by full-matrix least-squares methods). In the final cycles of refinement all non-hydrogen atoms were allowed anisotropic thermal parameters. Hydrogen atoms were placed in idealised positions with free isotropic thermal parameters. Refinement was completed with $R = R' = 0.038$ and R_g = 0.041[19] for all 2376 reflections, equally weighted. The largest peaks in a final difference map, with magnitude <0.6 e $Å^{-3}$, were all in the vicinity of the metal atom. Scattering factor curves for neutral atoms were taken from ref. 20. Computer programs used in the analysis have been noted above and in ref. 21, and were run on the MicroVAX II machine in this Laboratory.

trans-$[FeH(Br)(depe)_2]BPh_4$. *Crystal data.* $C_{20}H_{49}BrFeP_4 \cdot C_{24}H_{20}B$, M = 868.5, orthorhombic space group $P2_12_12_1$ (no. 19), a = 10.927(1), b = 16.109(2), c = 25.826(2) Å, U = 4546.0 $Å^3$, Z = 4, D_c = 1.269 g cm^{-3}, $F(000)$ = 1836, μ(Mo-Kα) = 13.7 cm^{-1}.

The examination and X-ray analysis of this sample followed closely those described above. On a beautiful, bright red prismatic crystal, *ca.* 0.28 × 0.31 × 0.36 mm, the quality of diffraction data allowed centring of reflections at θ *ca.* 14.5°, and measurement of intensities to θ_{max} of 23° (for reflections of positive indices h, k and l). There was slight deterioration of the crystal during the data collection (4.7% in intensity overall); corrections for this and the other effects were applied as before. Data for 3549 unique reflections were used in SHELX[19] and our extended version SHELXN[22] for structure determination and refinement. Hydrogen atoms of methylene and phenyl groups were included in idealised positions; those in methyl groups were identified in difference maps and included with geometrical restraints. The hydride ligand was located close to its expected site in the octahedral co-ordination sphere of the iron atom and was allowed to refine freely. All the non-hydrogen atoms were refined anisotropically. The thermal parameters for the ethyl group of C(43)/C(44) were large, indicating considerable motion or perhaps disorder (not resolved); the hydrogen atoms were not included for this group. At convergence of the large-block-matrix least-squares refinement, R = 0.055, R' = 0.051 and R_g = 0.055[16] for all 3549 reflections weighted $w = (\sigma_F^2 + 0.000\,565F^2)^{-1}$. There were no peaks of significance in the final difference map.

Refining the inverted structure (with coordinates $\bar{x}, \bar{y}, \bar{z}$) gave corresponding R factors of 0.074, 0.074 and 0.080. We believe therefore that the coordinates of Table 6 are for the correct conformation for the chosen crystal.

Additional material for both structures available from the Cambridge Crystallographic Data Centre comprises H-atom coordinates, thermal parameters and remaining bond lengths and angles.

Acknowledgements

We thank Colin Macdonald for microanalytical results and help with NMR spectroscopy.

References

1 J. K. Kochi, *Organometallic Mechanisms and Catalysis*, Academic Press, New York, 1978, ch. 14 and refs. therein.
2 M. Tamura and J. K. Kochi, *J. Organomet. Chem.*, 1971, **31**, 289.
3 R. B. Allen, R. G. Lawler and H. R. Ward, *J. Am. Chem. Soc.*, 1973, **95**, 1692.
4 D. J. Evans, M. Jimenez-Tenorio and G. J. Leigh, *J. Chem. Soc., Dalton Trans.*, 1991, 1785.
5 G. M. Bancroft, M. J. Mays and B. E. Prater, *J. Chem. Soc. A*, 1970, 956.
6 M. Gargano, P. Giannoccaro, M. Rossi, G. Vasapollo and A. Sacco, *J. Chem. Soc., Dalton Trans.*, 1975, 9.
7 J. E. Barclay, A. Hills, D. L. Hughes and G. J. Leigh, *J. Chem. Soc., Dalton Trans.*, 1988, 2871.
8 M. DiVaira, S. Midollini and L. Sacconi, *Inorg. Chem.*, 1981, **20**, 3430 and refs. therein.
9 J. Chatt and R. G. Hayter, *J. Chem. Soc.*, 1961, 5507.
10 R. H. Morris, J. F. Sawyer, M. Shiralian and J. D. Zubkowski, *J. Am. Chem. Soc.*, 1985, **107**, 5581.
11 J. S. Ricci, T. F. Koetzle, M. T. Bautista, T. M. Hofstede, R. H. Morris and J. F. Sawyer, *J. Am. Chem. Soc.*, 1989, **111**, 8823.
12 A. Hills, D. L. Hughes, M. Jimenez-Tenorio and G. J. Leigh, *J. Organomet. Chem.*, 1990, **391**, C41.
13 C. A. Ghilardi, S. Midollini, L. Sacconi and P. Stoppioni, *J. Organomet. Chem.*, 1981, **205**, 193.
14 C. L. Kwan and J. K. Kochi, *J. Am. Chem. Soc.*, 1976, **98**, 4903.
15 Ref. 1, ch. 13 and refs. therein.
16 G. S. Bodner, J. A. Gladysz, M. F. Nielsen and V. D. Parker, *J. Am. Chem. Soc.*, 1987, **109**, 1757 and refs. therein.
17 J. H. Espenson, *Advances in Inorganic and Bioinorganic Mechanisms*, ed. A. G. Sykes, Academic Press, New York, 1982, vol. 1, ch. 1 and refs. therein.
18 R. J. Burt, J. Chatt, W. Hussain and G. J. Leigh, *J. Organomet. Chem.*, 1979, **182**, 203.
19 G. M. Sheldrick, SHELX 76, Program for crystal structure determination, University of Cambridge, 1976.
20 *International Tables for X-Ray Crystallography*, Kynoch Press, Birmingham, 1974, vol. 4, pp. 99 and 149.
21 S. N. Anderson, R. L. Richards and D. L. Hughes, *J. Chem. Soc., Dalton Trans.*, 1986, 245.
22 G. M. Sheldrick, SHELXN, Extended version of SHELX, for refinement at up to 2000 atomic parameters, 400 atoms, University of Cambridge, 1977.

Received 5*th November* 1991; *Paper* 1/05615H